HHS Public Access

Author manuscript

Traffic. Author manuscript; available in PMC 2016 November 01.

Published in final edited form as:

Traffic. 2015 November ; 16(11): 1137–1154. doi:10.1111/tra.12314.

Endocytosis of ubiquitylation-deficient EGF receptor mutants via clathrin coated pits is mediated by ubiquitylation

Arola Fortian[*], **Lai Kuan Dionne**[†], **Sun Hae Hong**[‡], **Woong Kim**[§], **Steven P. Gygi**[§], **Simon Watkins**[*], and **Alexander Sorkin**[*]

[*]Department of Cell Biology, University of Pittsburgh School of Medicine, Pittsburgh, PA, USA

[†]University of Colorado Anschutz Medical Center, Aurora, CO USA

[‡]University of California at Berkeley, Berkeley, CA USA

[§]Department of Cell Biology, University of Harvard School of Medicine, Boston, MA, USA

Abstract

Signaling by EGF receptor (EGFR) is controlled by endocytosis. However, mechanisms of EGFR endocytosis remain poorly understood. Here we found that the EGFR mutant lacking known ubiquitylation, acetylation and clathrin adaptor AP-2 binding sites (21KRΔAP2) was internalized at relatively high rates via clathrin-dependent pathway in human duodenal adenocarcinoma HuTu-80 cells. RNA interference analysis revealed that this residual internalization is strongly inhibited by depletion of Grb2 and the E2 ubiquitin-conjugating enzyme UbcH5b/c, and partially affected by depletion of the E3 ubiquitin ligase Cbl and ubiquitin-binding adaptors, indicating that an ubiquitylation process is involved. Several new ubiquitin conjugation sites were identified by mass-spectrometry in the 21KRΔAP2 mutant, suggesting that cryptic ubiquitylation may mediate endocytosis of this mutant. Total internal reflection fluorescence microscopy imaging of HuTu-80 cells transfected with labeled ubiquitin adaptor epsin1 demonstrated that ubiquitylation-deficient EGFR mutant was endocytosed through a limited population of epsin-enriched clathrin coated pits (CCPs), although with a prolonged CCP lifetime. Native EGFR was recruited with the same efficiency into CCPs containing either AP-2 or epsin1 that were tagged with fluorescent proteins by genome-editing of MDA-MD-231 cells. We propose that two redundant mechanisms, ubiquitylation and interaction with AP-2, contribute to EGFR endocytosis via CCPs in a stochastic fashion.

Graphical Abstract

[*]Corresponding author: Alexander Sorkin, Department of Cell Biology, University of Pittsburgh School of Medicine, S368 Biomedical Science Tower South, 3500 Terrace Street, Pittsburgh, PA 15261, Phone: 412-6243116, FAX: 412-648-8330, sorkin@pitt.edu.

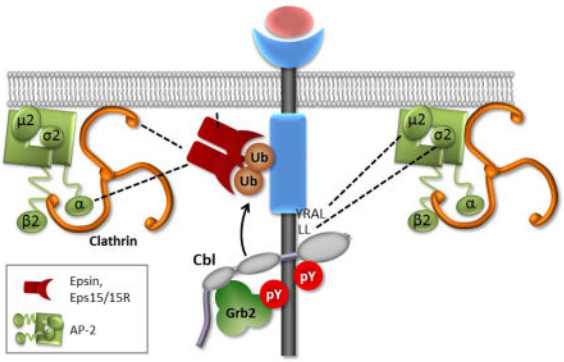

Keywords

EGF; endocytosis; ubiquitin; clathrin

Introduction

Epidermal growth factor receptor (EGFR) is the archetypical member of the large family of receptor tyrosine kinases. EGFR is important in eukaryotic development, regulation of adult cells in various tissues, and pathogenesis of cancer and other diseases (1). EGFR is activated at the cell surface by at least seven different ligands. Ligand binding leads to receptor dimerization, activation of its tyrosine kinase and phosphorylation of several tyrosines in the cytoplasmic domain of the receptor and other cytoplasmic proteins (2). Phosphorylated tyrosines serve to recruit enzymes or adaptors that link enzymes to the receptor, which results in activation of signaling cascades and culminates in cell proliferation, survival and motility.

Ligand-bound EGFR is also rapidly internalized via clathrin-mediated endocytosis (CME) and clathrin–independent endocytosis (CIE) pathways into endosomes where it is efficiently sorted to the lysosome-degradation pathway (3). Accelerated internalization and degradation of activated EGFR result in down-regulation of the EGFR protein and its activity. Endocytosis regulates not only the amount of active receptors but also the location of signaling processes (4). Despite the major role of endocytosis in the regulation of EGFR activity, mechanisms of EGFR endocytosis are not understood. Several mechanisms of clathrin-independent endocytosis of EGFR were proposed, including those mediated by Cbl-CIN85-endophilin interactions (5, 6), receptor ubiquitylation (7), and by di-leucine internalization motif and dimerization of EGFR (8). However, demonstration of EGFR internalization via these pathways requires high concentrations of EGF. Also, a receptor-kinase-independent mechanism of internalization involving extracellular juxta-membrane dimerization motif of EGFR was reported (9). Because concentrations of EGFR ligands accessible to the receptor in most normal mammalian tissues and tumors are low (< 1–2 ng/ml) (10–14), we focus on studying the clathrin-mediated and EGFR kinase-dependent internalization that is typically observed in experiments with cultured cells treated with low EGF concentrations.

Studies of various EGFR mutants expressed in porcine aortic endothelial (PAE) cells lacking endogenous EGFR led to a model whereby ubiquitylation of the EGFR kinase domain, clathrin adaptor AP-2 binding sites and several lysine residues in the C-terminus, that were found to be acetylated, are all involved in the CME of EGFR in a redundant fashion (15). Ubiquitylation of EGFR is mediated by the E3 ligase Cbl (c-Cbl and Cbl-b isoforms) that can directly bind to EGFR via phosphorylated Tyr1045 and indirectly through the interaction with the SH2-SH3 adaptor protein Grb2 that binds to phosphorylated Tyr1068 and Tyr1086 in the EGFR [(16,) reviewed in (3)]. Both modes of interaction are necessary for the full extent of EGFR ubiquitylation. Grb2 was shown to be essential for EGFR internalization through CME (17, 18). Elimination of 21 lysines in the kinase domain and C-terminus together with mutations of AP-2 binding motifs produced an EGFR mutant 21KRΔAP2 that has the residual internalization rate of 25–30% of that rate of the wild-type EGFR (wtEGFR) (15). This residual endocytosis was shown to be clathrin-dependent in PAE cells but its mechanism remains unknown.

To study the role of EGFR endocytosis in signaling, complete understanding of all endocytic mechanisms mediating EGFR internalization is necessary. To gain insight into the internalization mechanisms of the 21KRΔAP2 mutant, this mutant was expressed in human duodenal carcinoma HuTu-80 cells lacking endogenous EGFR. Interestingly, the 21KRΔAP2 mutant was more efficiently internalized in HuTu-80 cells when compared to PAE cells. siRNA screening combined with mass-spectrometry and total internal reflection fluorescence microscopy (TIR-FM) imaging of clathrin coated pit (CCP) dynamics suggested that an ubiquitylation event is involved in the residual endocytosis, likely, due to additional ubiquitylation of lysine residues remaining in the 21KRΔAP2 mutant. A new simplified model is proposed whereby two mechanisms (EGFR ubiquitylation and AP-2 binding) stochastically contribute to EGFR endocytosis via CCPs.

RESULTS

RNA interference screen reveals involvement of an ubiquitylation event in 21KRΔAP2 internalization

Human cells are far more amendable to an RNA interference analysis than porcine (PAE) cells because of the availability of well-characterized human gene targeted siRNAs. To study the mechanisms of CME of the 21KRΔAP2 EGFR mutant lacking 21 lysines and AP-2 binding internalization motifs (Figure 1A), this mutant and wtEGFR were stably expressed in human duodenal carcinoma HuTu-80 cells using retroviral-mediated transfection. Multiple single-cell clones (50–150 × 10^3/EGFRs per cell) were selected for further analysis to control for clonal variation. EGFR is widely expressed in various cells of the gastrointestinal tract; it is important for regulation of their normal proliferation and differentiation, as well as oncogenic transformation (19). HuTu-80 cells are a rear example of intestinal cells that do not express detectable amounts of the EGFR protein (Figure 1B) and display negligible binding of ^{125}I-EGF (data not shown). The extent of tyrosine phosphorylation of EGF-activated wtEGFR and 21KRΔAP2 was similar, indicative of a similar kinase activity (Figure 1B). The rate of wtEGFR internalization in HuTu-80 cells, measured using ^{125}I-EGF (1 ng/ml), was comparable to the rates that are typically observed

in various types of cells expressing endogenous or heterologous EGFR (internalization rate constant k_e ~ 0.2–0.25/min) (Figure 1C), confirming that these cells are an appropriate experimental system to study EGFR endocytosis. Surprisingly, the 21KRΔAP2 mutant was internalized in HuTu-80 cells at a relatively high rate, ~50–60% of the wtEGFR internalization rate (Figure 1C). Strong endosomal accumulation of the mutant receptor was observed in cells incubated with EGF-rhodamine (EGF-Rh) (Figure 1D). Significant residual internalization of the 21KRΔAP2 mutant underscores the importance of studying mechanisms underlying this internalization to fully understand the pathways regulating EGFR endocytosis.

To examine the mechanism of 21KRΔAP2 internalization, the effect of various siRNAs, that are targeting proteins with known or putative functions in CME and validated in previous studies (18, 20–25) on ^{125}I-EGF (1 ng/ml) internalization was tested (Figure 2). Experiments in which protein depletion was > 80% (Supplemental Materials, Figure S1A–F) were used for calculations of the mean effects of siRNAs on endocytosis. The internalization of both wtEGFR and 21KRΔAP2 was strongly inhibited by the EGFR kinase inhibitor PD158780 (Figure 2). Kinase-independent internalization rates of wtEGFR and the mutant EGFR were similar, thus representing the basal, constitutive endocytosis (k_e < 0.05/min). Similar to what was observed in PAE cells, the internalization rate of the 21KRΔAP2 mutant in HuTu-80 cells was decreased by clathrin heavy chain (CHC) knockdown to the level of kinase-independent internalization, suggesting that the 21KRΔAP2 mutant is internalized via CCPs (Figures 2A and B).

Grb2 depletion has also reduced internalization of 21KRΔAP2 to a minimal level. This result suggested that Grb2 associated proteins may directly link this EGFR mutant to a CCP or trigger biochemical reactions that mediate the recruitment of this mutant into CCP. Tom1L that is capable of binding to the SH2 domain of Grb2 was previously implicated in EGFR endocytosis (26). However, Tom1L knockdown did not affect wtEGFR or 21KRΔAP2 internalization in our experiments (Figure 2A). Since Grb2 depletion was shown to inhibit EGFR ubiquitylation (27), several siRNAs targeted to proteins involved in EGFR ubiquitylation and recognition of ubiquitin moieties were tested for the effect on endocytosis. Depletion of c-Cbl or both c-Cbl and Cbl-b partially inhibited endocytosis of the 21KRΔAP2 mutant (Figure 2A). It is likely that the strongest knockdown of Cbl below a minimal concentration sufficient for EGFR ubiquitylation is necessary to achieve a more efficient endocytosis inhibition. In contrast to c-Cbl knockdown, single knockdown of Cbl-b did not affect EGFR internalization, suggesting that c-Cbl is predominantly involved. Considering an alternative possibility that additional E3 ligases are involved, siRNA to NEDD4, an E3 implicated in endocytosis of receptor tyrosine kinases and other cargo (28, 29) was tested. However, depletion of NEDD4 did not affect 21KRΔAP2 internalization (Figure S1G) or produced an effect additional to Cbl depletion (data not shown), respectively. By contrast, siRNA to UbcH5b/c (UBE2D2/3), two highly homologous isoforms of the E2 ubiquitin-conjugating enzyme, strongly inhibited 21KRΔAP2 internalization (Figures 2A and C). UbcH5b/c is known to bind Cbl and participate in Cbl-mediated ubiquitylation of EGFR (23). Altogether, these data imply that an ubiquitylation reaction catalyzed by UbcH5b/c, and possibly, by Grb2-associated Cbl proteins, is involved in 21KRΔAP2 internalization.

Various combinations of siRNAs to eps15, eps15R, epsin1 and epsin2, CCP proteins containing ubiquitin-binding domains, partially inhibited 21KRΔAP2 internalization (Figure 2A). A possible explanation of partial effects is incomplete simultaneous depletion of these functionally redundant proteins. siRNA depletion of FCHo1 and FCHo2 had a strong inhibitory effect on 21KRΔAP2 internalization while only partially inhibited the internalization of wtEGFR. Whereas FCHo1/2 participate in the initial stage of CCP assembly, they are also a part of the ubiquitin recognition module through their association with Eps15 (22, 30). Therefore, increased sensitivity to FCHo1/2 depletion may further indicate the importance of ubiquitin-mediated mechanisms of 21KRΔAP2 endocytosis.

New ubiquitylation sites identified in the EGFR mutant by mass-spectrometry

While siRNA experiments implicated ubiquitylation in 21KRΔAP2 endocytosis, no ubiquitin signal, or faint smeared ubiquitin immunoreactivity in some experiments with clones expressing very high levels of mutant receptor could be detected in 21KRΔAP2 immunoprecipitates (Figure 3A). We first hypothesized that an unknown adaptor protein may mediate 21KRΔAP2 endocytosis. Such protein must (i) be associated with the 21KRΔAP2 mutant; (ii) be ubiquitylated in EGF- and Grb2/UbcH5-dependent manner; and (iii) directly/indirectly interact with the clathrin coat. Global analysis of ubiquitylated proteins using an enrichment of di-glycine (diGly) motif signature generated from tryptic peptides from ubiquitylated proteins using (di-Gly)-antibody (31) as well as search of the published data on EGFR-dependent/independent ubiquitinomes (32) did not yield a potential ubiquitylated adaptor that would satisfy all three criteria set above. However, using the same strategy of an antibody-based enrichment of diGly-modified tryptic peptides recovered from EGFR immunoprecipitates, new ubiquitylation sites were detected in 21KRΔAP2 (Figures 3B and C). In particular, ubiquitylation of Lys855 and Lys851 appeared to be EGF-dependent (Figure 3C). Ubiquitylation of Lys851was also detected in wtEGFR-expressing HuTu-80 in addition to previously mapped ubiquitylation sites. Ubiquitylation of Lys851 in wtEGFR was also observed in EGF-stimulated PAE cells (33) and head-and-neck squamous cell carcinoma SCC2 cells (data not shown). Figure 3B shows that Lys721 is the catalytic residue of the receptor kinase, while Lys851 and Lys855 are situated near the ATP binding pocket of the EGFR kinase. In fact, conserved mutations of lysines 704, 828, 851 and 855 to arginines were shown to inhibit the receptor kinase activity (34), which precluded functional testing of the role of these cryptic ubiquitylation sites in EGFR internalization. However, these experiments suggested that 21KRΔAP2 ubiquitylation itself, in particular, Lys851, rather than additional ubiquitylated adaptors, may mediate endocytosis of this EGFR mutant.

The potential involvement of ubiquitylation in 21KRΔAP2 internalization prompted the generation of a new mutant in which Cbl binding site Tyr1045 was mutated in the 21KRΔAP2 construct (Figure 1A). However, measurements of EGF internalization rates in several HuTu-80 clones stably expressing the 21KRΔAP2/Y1045F mutant revealed that Y1045F mutation did not further reduced the internalization rate of the 21KRΔAP2 mutant. This result suggested that direct Cbl binding to the Y1045F mutant is not necessary for its internalization.

CCP cycle dynamics during internalization of wild-type and mutant EGFR

To analyze how ubiquitylation regulates the CME of EGFR, the dynamics of the CCP lifecycle was analyzed using TIR-FM in HuTu-80 cells expressing wtEGFR or ubiquitin-deficient EGFR mutant. In these experiments we have chosen a 21KRΔAP2/Y1045F expressing cell clone with the slowest endocytosis (k_e = 0.082+/−0.007 min^{-1}) and the receptor density matching one of the wtEGFR-expressing clonal cells (clone B6).

To label CCPs, β2-subunit of AP-2 tagged with YFP (β2-YFP) or epsin1 tagged with Venus were transiently expressed in HuTu-80/wtEGFR and HuTu-80/21KRΔAP2/Y1045F cells. Expression of β2-YFP results in labeling the entire population of AP-2 containing clathrin coated structures through competitive replacement of the endogenous β2-subunit in the AP-2 complex by transfected β2-YFP, but does not result in the increased amounts of AP-2 in CCPs because other AP-2 subunits are not overexpressed (35). Overexpression of a monomeric adaptor, such as epsin1, likely increases the amount of this protein in CCPs, and therefore, increases the population of CCPs with a high capacity of recruiting the ubiquitylated cargo. Cells with the lowest detectable expression levels of β2-YFP or epsin1-Venus were used for TIR-FM. Control experiments using confocal imaging revealed that EGF-Rh endocytosis is unaffected by low-to-moderate expression levels of epsin1-Venus or β2-YFP (data not shown).

Treatment with EGF-Rh (2 ng/ml) at 37°C resulted in rapid binding of EGF-Rh to receptors mostly at the periphery of the bottom cell membrane in all experimental variants (Figure 4A). Only a minimal binding was observed in the central area of the cell where numerous large pleiomorphic structures containing labeled AP-2 or epsin1 were located. These structures were co-localized with clathrin (data not shown) and most likely represent flat clathrin lattices. EGF-Rh was found exclusively in diffraction-limited spots of AP-2 or epsin1, most probably single CCPs, but not in large labeled “plaques” (Figure 4A). We have shown in early studies that EGFR is recruited to CCPs mostly on the dorsal membrane and at the edges of NIH 3T3 cells (36). The lack of EGFR recruitment to the large clathrin structures on the bottom membrane was observed in several types of cells (37, 38) (also see Figures 6 and 7 below), although the molecular mechanisms of this spatial regulation of EGFR internalization are not understood.

The percentage of CCPs containing EGF-Rh reached a maximum at ~3 min after EGF-Rh stimulation and then gradually decreased (Figure 4B). At maximum both wtEGFR- and mutant-ligand complexes were clustered in ~10% of CCPs labeled with AP-2 (Figure 4B). By contrast with AP-2 marked CCPs, EGF-Rh was recruited to the twice lesser number of epsin1-labeled CCPs (~8% at maximum) in mutant EGFR-expressing cells than in wtEGFR-expressing cells (~15% at maximum) (Figure 4B). These data suggest that the most pronounced defect of the 21KRΔAP2/Y1045F mutant endocytosis is manifested in its recruitment into only a limited epsin1-enriched CCP population. However, loading of this mutant into this population of CCPs is readily detectable and substantial, despite a very low ubiquitylation level of the mutant.

To further examine the role of EGFR ubiquitylation in CCP cycle, the dynamics of co-localization of EGF-Rh and CCP proteins was followed in β2-YFP and epsin1-Venus

expressing cells during the full lifetime of the selected CCPs using TIR-FM microscopy. As shown on examples of the fluorescence intensity traces of EGF-Rh and β2-YFP or epsin1-Venus, EGF-Rh was recruited immediately at or soon after the initial appearance of YFP or Venus fluorescence spots (Figure 5A). We have not observed the recruitment of a CCP marker to a pre-existing EGF-Rh spot, suggesting that most EGFRs are recruited to a pre-existing CCPs or simultaneously with CCP nucleation. Because of weak EGF-Rh fluorescence signals in CCPs and a very small percent of CCPs containing both EGF-Rh and CCP markers that can be followed through the entire CCP cycle, analysis using automated software algorithms was not technically possible. Therefore, a double-blind manual analysis of traces of individual CCPs was performed as described in "Methods". Interestingly, averaged duration of the lifecycle of EGF-Rh internalizing CCPs, measured based on fluorescence traces of β2-YFP or epsin1-Venus, was, respectively, 55 sec or 50 sec in cells expressing wtEGFR whereas the mean life-time of CCPs internalizing EGF-Rh was significantly longer in cells expressing the 21KRΔAP2/Y1045F mutant (~80 sec) (Figure 5B). These data suggest that slow endocytosis of the EGFR mutant is due to the defects in both the cargo recruitment step and one of the later steps of the CCP cycle.

Dynamics of EGFR internalization through endogenously labeled CCPs

The results of experiments in HuTu-80 cells presented in Figures 2–5 supported previous EGFR mutagenesis and siRNA data (15) that implicated receptor ubiquitylation and recognition of ubiquitylated EGFR by CCP adaptors like epsins as one of the redundant mechanisms of EGFR internalization. To examine the relative contribution of ubiquitylation-dependent mechanisms in EGFR endocytosis without experimental manipulations, such as protein overexpression, depletion or mutagenesis, we examined CCP dynamics in MDA-MB-231 cells with endogenously labeled AP-2 and epsin1. To this end, cells that express μ2 subunit of AP-2 labeled with tagRFP.t (AP2-RFP) using TALE nuclease gene-editing (Hong et al., submitted for publication) were used to additionally label endogenous epsin1 with GFP. A pair of TALENs and a donor plasmid were created to insert tagGFP2 sequence into the N-terminus of the endogenous gene locus of epsin1 (Supplemental Materials, Figure S2A). Single cell clones (for example clone #17) were selected in which both epsin1 gene alleles were GFP-tagged as evident by the absence of untagged epsin1 (Figure S2B). Resulting MDA-MB-231/AP2/epsin-1-edited cells (further referred as MDA/AP2-RFP/GFP-EPN1 cells) internalized ^{125}I-EGF with the same rate as parental MDA-MB-231 cells suggesting that tagging μ2 and epsin1 with fluorescent proteins does not affect EGFR endocytosis (Figure 6A).

TIR-FM imaging demonstrated that similarly to HuTu-80 cells, large RFP and GFP labeled structures were concentrated in the middle of MDA/AP2-RFP/GFP-EPN1 cells, and diffraction-limited CCPs were predominantly seen at the periphery of the cell bottom membrane (Figure 6B). Approximately 400–2000 labeled structures were detected on the bottom membrane with the largest numbers of labeled structures in most flattened cells. Approximately 55–60% of labeled structures contained both AP2-RFP and GFP-epsin1 at steady-state growth conditions, and remaining 25–30% and 12–15% were labeled with, respectively, either AP2-RFP or GFP-epsin1. The fluorescence intensity of GFP-epsin1 containing structures was 5–10-tmes lower than that of AP2-RFP (after normalization to

apparent quantum yields), suggesting that epsin1 is a relatively minor component of the clathrin coat.

Stimulation of cells with EGF-Alexa647 (further referred as EGF-A647; 20 ng/ml) during continuous time-lapse imaging at 37°C resulted in rapid binding and clustering of the ligand in CCPs that reached maximum at ~ 4 min (Figures 6B and C). As in experiments with HuTu-80 cells, EGF-A647 was co-localized with diffraction-limited spots of AP2-RFP and GFP-epsin1 near cell edges, and was not found in large labeled plaques (clathrin lattices) in the middle of the cell (Figure 6B). By contrast, recruitment of another ligand, transferrin conjugated with Alexa647 (Trf-A647), into large clusters of AP-2 and epsin was readily detected in MDA/AP2-RFP/GFP-EPN1 cells by TIR-FM (Fig. 7), suggesting that the lack of EGF in these structures is not due to the poor ligand accessibility. 3D confocal imaging confirmed predominant recruitment of EGF-A647 into coated pits on the dorsal cell surface and localization of Trf-A647 in both dorsal and ventral AP2-labeled structures (Supplemental Materials, Figure S3).

The time-course of the percent of CCPs labeled with AP2-RFP that were co-localized with EGF-A647 was similar to that time-course of EGF-A647 containing GFP-epsin1 labeled CCPs (Supplemental Figure S2C), which was expected because most CCPs contained both AP2-RFP and GFP-epsin1. Importantly, the time course of EGF-A647 co-localization with labeled CCP presented in Figure 6C demonstrates that EGF-A647 was recruited to a similar population of CCPs that were singularly labeled with either AP2-RFP or GFP-epsin1 (Figure 6C). These data suggest that ligand-occupied EGFRs enter CCPs containing each of these adaptors with a similar efficiency.

The analysis of fluorescence traces of A647, GFP and RFP during the full lifetime of individual CCPs in MDA/AP2-RFP/GFP-EPN1 cells is presented in Fig. 6D. The lifetime of CCPs internalizing EGF-A647, that was measured based on the AP2-RFP traces exemplified in Figure 6D, was 60 ± 29 (S.D.) sec, a value similar to that measured in cells not treated with EGF-A647 (60 ± 33 sec). These data suggest that EGFR loading does not influence the dynamics of CCP cycle.

DISCUSSION

Our previous studies led to a complex model of the CME of EGFR involving at least four redundant mechanisms and resulted in the generation of the first internalization-impaired EGFR mutant (21KRΔAP2) with normal kinase activity (15). In order to fully understand the EGFR endocytic system, in the present study we investigated the mechanism of the substantial residual CME of such EGFR mutants in human carcinoma cells. We provide several lines of evidence for the unexpected role of ubiquitylation in this residual endocytosis of the ubiquitylation-deficient EGFR mutants.

First, the strong inhibition of the 21KRΔAP2 mutant endocytosis by siRNA knockdown of the E2 enzyme, UbcH5b/c, directly demonstrates the involvement of an ubiquitylation event in this endocytosis process. The precise role of UbcH5b/c is however unclear. While this enzyme is known to participate in Cbl-mediated ubiquitylation of EGFR through binding to

the RING domain of Cbl (23), depletion of Cbl proteins resulted only in a partial inhibition of internalization (Figure 2). It is possible that a very small level of c-Cbl/Cbl-b in depleted cells is sufficient for receptor internalization. Another possibility is that additional E3 ligases, other than Cbls and NEDD4, are involved in the EGFR-relevant UbcH5b/c catalyzed ubiquitylation reaction. UbcH5b/c may also be involved in ubiquitylation of Eps15 and epsin (39); however, this ubiquitylation most likely accelerates their turnover rather than promotes endocytosis.

Second, essential function of Grb2 in the internalization of the 21KRΔAP2 mutant in HuTu-80 (Figure 2) and PAE cells (15) further supports the role of ubiquitylation in this process. Certainly, Grb2 interacts with a number of SH2 and SH3 domain-binding proteins. Our experiments ruled out the involvement of Tom1L (Figure 2), and our previous work suggested no endocytic role for Grb2-SOS interactions (27). Because none of other previously-identified Grb2 interactors except Cbl are known to participate in ubiquitylation, the involvement of Grb2 in the 21KRΔAP2 mutant endocytosis is likely through binding to Cbl or another unidentified E3 ubiquitin ligase.

Third, the inhibitory effects of siRNAs to CCP proteins involved in the recognition of ubiquitylated cargo confirm the role of ubiquitylation in the internalization of the EGFR mutant. Certainly, epsins, Eps15/R and FCHo1/2 are involved in the assembly of the protein interaction network that controls the CCP lifecycle, and therefore, their depletion may affect the general CME process. However, a relatively strong impact of the combined depletion of these proteins, in particular FCHo1/2, on EGF endocytosis in the mutant-expressing cells (Figure 2) suggests that the ubiquitin-adaptor function of the epsin-Eps15-FCHo module has the major contribution in the 21KRΔAP2 receptor endocytosis.

Finally, the discovery of new ubiquitylation sites in EGFR suggests the possibility that cryptic ubiquitylation may mediate internalization of the ubiquitylation-deficient EGFR mutants, although as noted above the role of newly identified ubiquitin conjugation sites in internalization could not be formally proven by mutagenesis. An intriguing implication of the finding that several lysines that are important for kinase activity can be ubiquitylated is the possibility that attachment of an ubiquitin moiety to these residues may result in inactive kinase. It should be emphasized that ligand-activated EGFR represents a mixture of heterogeneously ubiquitylated species. Each active wtEGFR molecule is ubiquitylated at one or two sites (33), and therefore, each major conjugation site is occupied in only a fraction (at maximum 10–20%) of activated receptor. Based on the comparison of the number of ubiquitylated peptides recovered from wild-type and mutant EGFR (Supplemental Dataset), we estimate that approximately 10–15% of ligand-occupied mutant EGFR is ubiquitylated under conditions of our experiments. Furthermore, mass-spectrometry analysis of diGly-antibody enriched tryptic peptides recovered from lysates of SCC2 cells that express very high levels of EGFR yielded additional ubiquitin conjugation sites in the C-terminus of EGFR, Lys1037 and Lys1164 (data not shown). These lysines are mutated in 21KRΔAP2 and, therefore, this finding does not add to the understanding of the internalization mechanism of this mutant. In the same time, it suggests a possibility that the role of C-terminal lysines in wtEGFR endocytosis is due to their ubiquitylation rather than acetylation,

whereas acetylation may compete with ubiquitylation and/or regulate the receptor kinase activity as previously hypothesized (15).

To better understand the contribution of ubiquitylation in EGFR endocytosis, we analyzed the dynamics of EGFR-containing CCPs labeled with ubiquitin adaptor epsin1 and/or the most abundant CCP adaptor AP-2. Analysis of the CCP dynamics using TIR-FM in HuTu-80 cells demonstrated that the primary defect responsible for reduced internalization rates of the 21KRΔAP2 mutant is at the CCP recruitment step and an additional defect is the delayed completion of the CCP lifecycle (Figure 5). Prolonged CCP lifetime was observed when non-ubiquitylated opioid receptor was loaded into CCP which led to an idea of the ubiquitin-dependent “checkpoint” in the CCP cycle (40). However, the delay in coat scission by the ubiquitylation-deficient EGFR mutant was significantly smaller than that observed in the latter study, indicative of the distinct mechanisms underlying these CCP scission delays.

The amount of epsin per CCP was increased in cells overexpressing epsin1, which was evident from the observation that the fluorescence intensity of endogenous GFP-epsin1 spots in MDA/AP-2/GFP-EPN1 cells was 5–10-times lower than that of spots labeled with epsin1-Venus that was transiently expressed at low-moderate levels in HuTu-80 cells. Such increased epsin concentration would result in an elevated recruitment capacity for the ubiquitylated cargo of these CCPs in epsin-overexpressing cells. Therefore, considerable efficiency of the recruitment of the 21KRΔAP2/Y1045F mutant into epsin1-enriched pits (Figure 4) supports an unexpected role of ubiquitin-based recognition in the internalization of the ubiquitylation-deficient EGFR mutant.

Development of gene-edited MDA-MD-231 cells expressing endogenous EGFR and endogenously labeled AP-2 and epsin1 allowed us to begin the dissection of CME mechanisms without experimental manipulations, such as receptor mutagenesis, protein overexpression or knockdowns. The ability of EGFR to cluster in epsin-containing CCPs that lack AP-2 or contain very small amounts of AP2-RFP undetectable by TIR-FM directly demonstrates that ubiquitin moieties of EGFR may mediate its CCP recruitment. Likewise, CCPs that do not contain detectable amounts of GFP-epsin1 may contain epsin2 or epsin3, although we have been unable to detect these epsin species by western blotting.

Despite many years of extensive EGFR research, the CCP dynamics of EGF/EGFR and characteristics of the CCP cycle during EGFR internalization has not been studied. Our measurements yielded the lifetime of ~1 min for CCPs that internalize EGFR, a value commonly reported in studies of CCP dynamics (41, 42). Interestingly, μ-opioid receptor loading to CCP was found to prolong the CCP lifetime by increasing the dwell time of dynamin in the CCP (43). In our TIR-FM analysis wtEGFR recruitment did not change the lifetime of AP-2 or epsin suggesting that EGFR does not actively control CCP dynamics.

In summary, the present studies of EGFR endocytosis and CCP dynamics prompted us to revise our previous model of the CME of EGFR that assumed at least four redundant mechanisms to be involved (15) and led to a “simplified” model whereby two mechanisms, receptor ubiquitylation and interactions with AP-2, mediate EGFR recruitment into CCP and endocytosis. We hypothesize that EGFR has a similar propensity of interacting with CCP

proteins through ubiquitin moieties or AP-2 binding motifs. We further suggest that the relative contribution of these mechanisms may depend on the relative stoichiometry of ubiquitin adaptors and AP-2 in CCP and may, therefore, be cell-type specific.

MATERIALS AND METHODS

Reagents

Human recombinant EGF was from BD Bioscience. EGF-Rh, EGF-A647 and Trf-A647 were purchased from Invitrogen (Carlsbad, California, USA). PD158780 was purchased from Calbiochem. Other chemicals were from Sigma or Thermo Fisher Scientific unless indicated otherwise.

Monoclonal antibody to phosphotyrosines (PY20) conjugated to horseradish peroxidase (HRP), and monoclonal antibody to c-Cbl (#610442) were from BD Transduction Laboratories (San Diego, CA, USA); rabbit polyclonal antibodies to EGFR (1005), Grb2, Cbl-b (H-454) and epsin1 (H-130), and goat polyclonal antibody to epsin2 (C-16), NEDD4 (A-16) and UbcH5b/c (C-15) were from Santa Cruz Biotechnology (Santa Cruz, CA, USA); monoclonal antibody 528 to EGFR (mAb528) was from American Type Culture Collection (Manassas, VA, USA); monoclonal mouse antibody to EGFR phosphotyrosine 1068 (pY1068) was from Cell Signaling Technology (Beverly, MA, USA). Polyclonal rabbit antibodies to Eps15 (577) and Eps15R (860) were kindly provided by Dr. P. P. Di Fiore (European Institute of Oncology, Milan, Italy). Rabbit polyclonal antibody to CHC was from Abcam. Rabbit monoclonal antibody to Tom1L was from Epitomics (#0405). Rabbit polyclonal antibodies to FCHo1 and FCHo2 were a gift from Dr. Linton Traub (University of Pittsburgh). Rabbit polyclonal antibody to actin was from Sigma.

Cell culture and generation of stably transfected cell lines

HuTu-80 were grown in DMEM containing 5% FBS. To generate cells stably expressing wtEGFR or EGFR mutants, retroviral mediated protein expression was employed. Phoenix-Ampho packaging cells were plated at 10^6 cells/60-mm dishes and transfected with the PCL Ampho packaging vector and the pBABE oncogene plasmid containing an EGFR construct using the Effectene Kit according to manufacturer's protocol (Qiagen). At 24-h post-transfection, the medium was replaced with fresh DMEM containing 5%FBS, and the cells were grown for additional 24 hrs. The conditioned medium containing recombinant retroviruses was collected and filtered through 0.45 μm-pore-size polysulfonic filters. Aliquots of these supernatants were applied immediately to HuTu-80 cells. Polybrene (Sigma, St. Louis, MO, USA) was added to a final concentration of 8 μg/ml, and the cells were incubated for 12 hrs and then 6 hrs more in fresh growth medium. Single cell clones were selected in the presence of 1 μg/ml puromycin.

TALENs and donor design

TALENs were designed to cut ~7bp downstream of the start codon of the *EPN1* gene locus. TALENs were constructed following the protocol in (44). In short, monomers specific for target sequences were linked together by an iterative Golden Gate cloning strategy. TagGFP2-epsin1 donor plasmid was created by inserting the fluorescent protein coding

sequences followed by AGSTG linker at the start codon of the *EPN1* gene. A 1.7kb homology region of *EPN1* centered at the start codon in exon 1 was amplified from the genomic DNA of SK-MEL-2 cells with NdeI and SpeI restriction sites at the ends by Phusion polymerase (New England Biolabs, Ipswich, MA, USA). This homology region was inserted into the pCR8 backbone to create pCR8-EPN1 plasmid. The entire pCR8-*EPN1* plasmid was amplified to insert a BamHI restriction site at the start codon. TagGFP2 coding sequences were amplified with a linker AGSGT at the C-terminus and BamHI restriction sites at either end. The fluorescent protein coding sequences were inserted at the BamHI restriction site of pCR8-*EPN1* plasmid. Sequences were verified by PCR and sequencing. For a detailed protocol see (45).

Generation of genome-edited cell line

2μg of plasmids expressing TALENs and 20μg of donor plasmids were transfected into cells using a single cuvette Amaxa Nucleofector device (Lonza, Basel, Switzerland) following the manufacture's protocol. MDA-MB-231 cells grown in DMEM:F12 (1:1) containing 10% FBS and L-glutamine-penicillin-Streptomycin to ~80% confluency were harvested by trypsinization, resuspended in Nucleofector solution V, and transfected using Amaxa Nucleofector program X-013 (Lonza, Basel, Switzerland). After transfection, cells were grown at 37°C and 5% CO2 for recovery and proliferation. After 5–7 days, cells were trypsinized and sorted for GFP-positive signals as single cells directly into 96-well plates using a DAKO-Cytomation MoFlo High Speed Sorter (Glostrup, Denmark). Each clonal population was tested by fluorescence microscopy, genotyping and western blotting to identify true positive clones (Fig S2). Primers used for diagnostic PCR are EPN1-cel1-f: TTGTGTTTCCAGAGGTCCTCTTCCC, EPN1-cel1-r: TCGTGGCCTCTCGAACCTTGATC, and tGFP2-f: AACTTCAAGACCCGCCACAACA.

DNA constructs and cell transfection

Point mutations in the 21KRΔAP2 construct (15) were made using the QuickChange mutagenesis kit (Stratagene Cloning Systems (La Jolla, CA, USA) according to the manufacture protocol. The sense oligonucleotides used for 21KRΔAP2/Y1045F mutant was: 5′-AGCTTCTTGCAGCGATTCAGCTCAGACCCCACAGGC - 3′. β2 subunit of AP-2 tagged with YFP (β2-YFP) was characterized previously (36). Epsin1-Venus construct was a kind gift from Dr. Xiaowei Zhuang (Howard Hughes Medical Institute, Harvard Medical School) (46). HuTu-80 cells stably expressing wtEGFR or 21KRΔAP2/Y1045F mutant were transfected with Venus-Epsin1 or β2-YFP constructs using an Effectene kit.

RNA interference

Following siRNA duplexes were described and characterized in our previous work: CHC (20); Grb2 (15); c-Cbl and Cbl-b (21); Eps15, eps15R, epsin1 (20, 25); UbcH5b/c (28); NEDD4 (24); Tom1L (on-Targetplus SMARTpool cat#146691) (15). siRNA to epsin2 was described in (47); siRNA (on-Targetplus SMARTpools) to FCHo1 and FcHo2 were from Dharmacon (Thermo Scientific). Non-targeting siRNA was from Qiagen. The protocols of siRNA transfections are described in studies above. Typically, cells were used for

experiments 3 days after single siRNA transfection or 4 days after first siRNA transfection if the second transfection two days after the first transfection was performed.

Immunoprecipitation and Western blotting

To probe for active EGFR, cells in 100-mm plates were serum-starved overnight, treated with EGF at 37°C for indicated times, washed in ice-cold Ca^{2+}, Mg^{2+}-free PBS (CMF-PBS) and lysed in Triton X-100/Glycerol/Hepes solubilization buffer containing 1 mM ortho-vanadate and 10 mM N-ethyl-maleimide (15). EGFR was immunoprecipitated with mAb528 as described (15). The lysates and immunoprecipitates were resolved by 7.5% SDS-polyacrylamide gel electrophoresis (SDS-PAGE) followed by transfer to the nitrocellulose membrane. To test the efficiency of siRNA knockdowns, cells in 6-well dishes were lysed and electrophoresed as described above. Western blotting was performed with appropriate primary and secondary antibodies conjugated to far-red fluorescent dyes (IRDye-680 and -800) followed by detection using Odyssey LI-COR system. Quantifications were performed using LI-COR software. For blotting with PY20-HRP antibody, enhanced luminescence detection kit form Pierce was used as described (15).

EGF internalization

Mouse receptor-grade EGF (Collaborative Research, Inc., Bedford, MA, USA) was iodinated as described (48). In most experiments, the time course of ^{125}I-EGF (1 ng/ml) internalization was obtained to calculate the specific internalization rate constant k_e as the linear regression coefficient of the dependence of the ratio of internalized/surface ^{125}I-EGF against time as described (48). In a limited number of experiments the ratio of internalized/surface ^{125}I-EGF was determined at the 6-min time point with multiple replicates, and the value of k_e was calculated by dividing this ratio by 6. The low concentration of ^{125}I-EGF was used to avoid saturation of the clathrin-mediated internalization pathway. The amount of surface ^{125}I-EGF binding sites per cell was determined using ^{125}I-EGF binding assay at 4°C as described (48).

Mass-spectrometry

HuTu-80 cells stably expressing wtEGFR or mutant EGFR grown in 150-mm dishes were untreated or treated with 20 ng/ml EGF for 5 min at 37°C, washed with cold CMF-PBS and lysed in Triton X-100/glycerol/Hepes solubilization buffer containing 1% sodium deoxycholate, 1mM ortho-vanadate and 10 mM N-ethyl-maleimide as described (33). EGFR was immunoprecipitated with mAb528 antibody, and the precipitates were washed with 0.5M NaCl to minimize co-precipitation of other proteins. Proteins were eluted from Protein A-agarose beads by boiling in the sample buffer without bromophenol blue, and then precipitated using the methanol-chloroform method (49). The precipitates were digested with trypsin and enriched using ubiquitin remnant motif antibody K-ε-GG (Cell Signaling Technology) as described (31). Peptides eluted from the diGly-antibody were analyzed by LC-MS/MS on an LTQ Orbitrap Velos, and the localization of each diGly site was evaluated as described (31). The list of diGly-modified peptides and spectra are presented in the Supplemental Materials.

Spinning disk confocal microscopy

HuTu-80 and MDA-MD-231 cells plated on 35 mm collagen-coated glass bottom plates (Mat-Tek, Ashland, MA) were serum starved for 16 h, and incubated with EGF-Rh, EGF-A647 or Tfr-A647 (precleared by centrifugation) for indicated times at 37°C. Cells were washed with ice-cold phosphate buffer saline (PBS) and fixed with freshly prepared 4% para-formaldehyde. Cell nuclei were stained with 4′,6-Diamidino-2-phenylindole (DAPI; 10 min) before coverslips were mounted on slides with Pro-Long Gold antifade reagent (Invitrogen). Z-stacks of 16–40 serial confocal images (200–500 nm intervals) were acquired through DAPI, 488nm (GFP), 561 nm (RFP and rhodamine) and 640 nm (Alexa647) channels and analyzed using a spinning disk confocal imaging system (Intelligent Imaging Innovation, Denver, CO) as described (50).

TIR-FM imaging

HuTu-80 and MDA-MB-231 cells were serum-starved for 16 hrs. For two- and three-color TIR-FM, cells in Mat-Tek dishes were imaged on a Nikon Eclipse Ti inverted microscope (Nikon, Melville, NY, USA) with a 100 × 1.49 NA oil-immersion objective using 488 nm, 561 nm and 640 nm laser lines, and with 5 sec intervals between time frames. All experiments were performed at 37°C in DMEM (HuTu-80) or DMEM:F12 (1:1) (MDA-MB-231) containing 0.1% BSA, 10mM HEPES, pH7.2. EGF-Rh, EGF-A647 or Trf-A647 were added during continuous image acquisition. Images were collected using Nikon Elements software (version 4.30, Nikon, Melville, NY) and an Andor (Belfast, Ireland) Zyla 5.5 camera; at full resolution under these conditions the pixel size with a 1 × coupler matches Nyquist sampling (120 nm xy exactly).

TIR-FM image analysis

Image analysis was performed using Imaris 7.1 software (Bitplane INC, South Windsor, CT). Images were thresholded, and particle tracking function was used to define and quantify co-localization of CCP markers and ligands. After automatic detection of particles with an estimated diameter of <450 nm, particles were filtered by quality control parameters (maximal travel distance, track duration, track displacement length, trace gap size). Appropriate threshold values were confirmed by visual inspection of correct particle detection. Brownian motion particle-tracking algorithm was applied to trace objects through sequential frames. The maximum permissible gap length implemented on the algorithm applied was no more than 3 frames to track segments interrupted by the temporary disappearance of particles.

The total number of CCP spots (AP-2 and/or epsin1) and spots with co-localized CCP proteins and labeled EGF (defined as 70% of spots overlap) on the cell-bottom membrane were calculated at each time point using Imaris. The percent of AP-2 or epsin labeled spots containing labeled EGF relative to the total number of detected structures labeled with AP-2 or epsin1 was then calculated in single cells. Mean percentages from 10 to 13 cells (on average of 3000–6000 CCPs) per an experimental condition were calculated and plotted against time.

Nikon Elements software (version 4.30, Nikon, Melville, NY) was used to generate time series of images of single CCP spots and corresponding kymographs, as well as traces of the fluorescence intensities of labeled EGF and CCP markers during the full life cycle of single CCPs. The lifetime of CCP was measured as the time between the first time point of the appearance of CCP marker spot (15% increase of fluorescence intensity above background) and the last time point of the same spot (fluorescence intensity 15% higher than background) (scission event). Only cases in which the traces of fluorescence of CCP markers and the ligand simultaneously decreased to a background level were used for calculations.

Statistical analysis

Statistical significance (P value) was calculated using unpaired two-tailed Student's t tests (Prism 5 and Excel).

Supplementary Material

Refer to Web version on PubMed Central for supplementary material.

Acknowledgments

We thank Drs. Linton Traub and Paolo Di Fiore for their kind gifts of antibodies, and Dr. Xiaowei Zhuang for the gift of epsin1-Venus construct. We are also grateful to Dr. David Drubin (University of California Berkeley) for providing MDA-MD-231/AP2-RFP genome-edited cells. This work was supported by the NIH/NCI CA089151 grant.

Abbreviations

A647	Alexa647
CCP	clathrin coated pit
CHC	clathrin heavy chain
CIE	clathrin independent endocytosis
CME	clathrin mediated endocytosis
diGly	di-glycine
EGFR	EGF receptor
TIR-FM	total internal reflection fluorescence microscopy
Tfr-A647	transferrin-Alexa647
wtEGFR	wild-type EGFR

References

1. Sibilia M, Kroismayr R, Lichtenberger BM, Natarajan A, Hecking M, Holcmann M. The epidermal growth factor receptor: from development to tumorigenesis. Differentiation. 2007; 75(9):770–787. [PubMed: 17999740]
2. Lemmon MA, Schlessinger J. Cell signaling by receptor tyrosine kinases. Cell. 2010; 141(7):1117–1134. [PubMed: 20602996]

3. Sorkin A, Goh LK. Endocytosis and intracellular trafficking of ErbBs. Exp Cell Res. 2009; 315(4): 683–696. [PubMed: 19278030]
4. Sigismund S, Confalonieri S, Ciliberto A, Polo S, Scita G, Di Fiore PP. Endocytosis and signaling: cell logistics shape the eukaryotic cell plan. Physiological reviews. 2012; 92(1):273–366. [PubMed: 22298658]
5. Soubeyran P, Kowanetz K, Szymkiewicz I, Langdon WY, Dikic I. Cbl-CIN85-endophilin complex mediates ligand-induced downregulation of EGF receptors. Nature. 2002; 416(6877):183–187. [PubMed: 11894095]
6. Boucrot E, Ferreira AP, Almeida-Souza L, Debard S, Vallis Y, Howard G, Bertot L, Sauvonnet N, McMahon HT. Endophilin marks and controls a clathrin-independent endocytic pathway. Nature. 2015; 517(7535):460–465. [PubMed: 25517094]
7. Sigismund S, Woelk T, Puri C, Maspero E, Tacchetti C, Transidico P, Di Fiore PP, Polo S. From the Cover: Clathrin-independent endocytosis of ubiquitinated cargos. Proc Natl Acad Sci U S A. 2005; 102(8):2760–2765. [PubMed: 15701692]
8. Wang Q, Chen X, Wang Z. Dimerization drives EGFR endocytosis through two sets of compatible endocytic codes. J Cell Sci. 2015; 128(5):935–950. [PubMed: 25588832]
9. Heukers R, Vermeulen JF, Fereidouni F, Bader AN, Voortman J, Roovers RC, Gerritsen HC, van Bergen En Henegouwen PM. Endocytosis of EGFR requires its kinase activity and N-terminal transmembrane dimerization motif. J Cell Sci. 2013; 126(Pt 21):4900–4912. [PubMed: 23943881]
10. Hirata Y, Orth DN. Epidermal growth factor (urogastrone) in human tissues. The Journal of clinical endocrinology and metabolism. 1979; 48(4):667–672. [PubMed: 219006]
11. Mutsaers AJ, Francia G, Man S, Lee CR, Ebos JM, Wu Y, Witte L, Berry S, Moore M, Kerbel RS. Dose-dependent increases in circulating TGF-alpha and other EGFR ligands act as pharmacodynamic markers for optimal biological dosing of cetuximab and are tumor independent. Clin Cancer Res. 2009; 15(7):2397–2405. [PubMed: 19276250]
12. Oka Y, Orth DN. Human plasma epidermal growth factor/beta-urogastrone is associated with blood platelets. The Journal of clinical investigation. 1983; 72(1):249–259. [PubMed: 6603475]
13. Yagi H, Miyamoto S, Tanaka Y, Sonoda K, Kobayashi H, Kishikawa T, Iwamoto R, Mekada E, Nakano H. Clinical significance of heparin-binding epidermal growth factor-like growth factor in peritoneal fluid of ovarian cancer. Br J Cancer. 2005; 92(9):1737–1745. [PubMed: 15827558]
14. Yamane S, Ishida S, Hanamoto Y, Kumagai K, Masuda R, Tanaka K, Shiobara N, Yamane N, Mori T, Juji T, Fukui N, Itoh T, Ochi T, Suzuki R. Proinflammatory role of amphiregulin, an epidermal growth factor family member whose expression is augmented in rheumatoid arthritis patients. J Inflamm (Lond). 2008; 5:5. [PubMed: 18439312]
15. Goh LK, Huang F, Kim W, Gygi S, Sorkin A. Multiple mechanisms collectively regulate clathrin-mediated endocytosis of the epidermal growth factor receptor. J Cell Biol. 2010; 189(5):871–883. [PubMed: 20513767]
16. Levkowitz G, Waterman H, Ettenberg SA, Katz M, Tsygankov AY, Alroy I, Lavi S, Iwai K, Reiss Y, Ciechanover A, Lipkowitz S, Yarden Y. Ubiquitin ligase activity and tyrosine phosphorylation underlie suppression of growth factor signaling by c-Cbl/Sli-1 [In Process Citation]. Mol Cell. 1999; 4(6):1029–1040. [PubMed: 10635327]
17. Waterman H, Katz M, Rubin C, Shtiegman K, Lavi S, Elson A, Jovin T, Yarden Y. A mutant EGF-receptor defective in ubiquitylation and endocytosis unveils a role for Grb2 in negative signaling. Embo J. 2002; 21(3):303–313. [PubMed: 11823423]
18. Jiang X, Huang F, Marusyk A, Sorkin A. Grb2 Regulates Internalization of EGF Receptors through Clathrin-coated Pits. Mol Biol Cell. 2003; 14(3):858–870. [PubMed: 12631709]
19. Fiske WH, Threadgill D, Coffey RJ. ERBBs in the gastrointestinal tract: recent progress and new perspectives. Experimental cell research. 2009; 315(4):583–601. [PubMed: 19041864]
20. Huang F, Khvorova A, Marshall W, Sorkin A. Analysis of clathrin-mediated endocytosis of epidermal growth factor receptor by RNA interference. J Biol Chem. 2004; 279(16):16657–16661. [PubMed: 14985334]
21. Huang F, Kirkpatrick D, Jiang X, Gygi S, Sorkin A. Differential regulation of EGF receptor internalization and degradation by multiubiquitination within the kinase domain. Mol Cell. 2006; 21(6):737–748. [PubMed: 16543144]

22. Umasankar PK, Sanker S, Thieman JR, Chakraborty S, Wendland B, Tsang M, Traub LM. Distinct and separable activities of the endocytic clathrin-coat components Fcho1/2 and AP-2 in developmental patterning. Nat Cell Biol. 2012; 14(5):488–501. [PubMed: 22484487]

23. Umebayashi K, Stenmark H, Yoshimori T. Ubc4/5 and c-Cbl Continue to Ubiquitinate EGF Receptor after Internalization to Facilitate Polyubiquitination and Degradation. Mol Biol Cell. 2008; 19(8):3454–3462. [PubMed: 18508924]

24. Vina-Vilaseca A, Bender-Sigel J, Sorkina T, Closs EI, Sorkin A. Protein kinase C-dependent ubiquitination and clathrin-mediated endocytosis of the cationic amino acid transporter CAT-1. The Journal of biological chemistry. 2011; 286(10):8697–8706. [PubMed: 21212261]

25. Sorkina T, Miranda M, Dionne KR, Hoover BR, Zahniser NR, Sorkin A. RNA interference screen reveals an essential role of Nedd4-2 in dopamine transporter ubiquitination and endocytosis. J Neurosci. 2006; 26(31):8195–8205. [PubMed: 16885233]

26. Liu NS, Loo LS, Loh E, Seet LF, Hong W. Participation of Tom1L1 in EGF-stimulated endocytosis of EGF receptor. EMBO J. 2009; 28(22):3485–3499. [PubMed: 19798056]

27. Huang F, Sorkin A. Growth Factor Receptor Binding Protein 2-mediated Recruitment of the RING Domain of Cbl to the Epidermal Growth Factor Receptor Is Essential and Sufficient to Support Receptor Endocytosis. Mol Biol Cell. 2005; 16(3):1268–1281. [PubMed: 15635092]

28. Vina-Vilaseca A, Sorkin A. Lysine 63-linked polyubiquitination of the dopamine transporter requires WW3 and WW4 domains of Nedd4-2 and UBE2D ubiquitin-conjugating enzymes. J Biol Chem. 2010; 285(10):7645–7656. [PubMed: 20051513]

29. Persaud A, Alberts P, Mari S, Tong J, Murchie R, Maspero E, Safi F, Moran MF, Polo S, Rotin D. Tyrosine phosphorylation of NEDD4 activates its ubiquitin ligase activity. Sci Signal. 2014; 7(346):ra95. [PubMed: 25292214]

30. Henne WM, Boucrot E, Meinecke M, Evergren E, Vallis Y, Mittal R, McMahon HT. FCHo proteins are nucleators of clathrin-mediated endocytosis. Science. 2010; 328(5983):1281–1284. [PubMed: 20448150]

31. Kim W, Bennett EJ, Huttlin EL, Guo A, Li J, Possemato A, Sowa ME, Rad R, Rush J, Comb MJ, Harper JW, Gygi SP. Systematic and quantitative assessment of the ubiquitin-modified proteome. Mol Cell. 2011; 44(2):325–340. [PubMed: 21906983]

32. Argenzio E, Bange T, Oldrini B, Bianchi F, Peesari R, Mari S, Di Fiore PP, Mann M, Polo S. Proteomic snapshot of the EGF-induced ubiquitin network. Molecular systems biology. 2011; 7:462. [PubMed: 21245847]

33. Huang F, Zeng X, Kim W, Balasubramani M, Fortian A, Gygi SP, Yates NA, Sorkin A. Lysine 63-linked polyubiquitination is required for EGF receptor degradation. Proc Natl Acad Sci U S A. 2013; 110(39):15722–15727. [PubMed: 24019463]

34. Huang F, Goh LK, Sorkin A. EGF receptor ubiquitination is not necessary for its internalization. Proc Natl Acad Sci U S A. 2007; 104(43):16904–16909. [PubMed: 17940017]

35. Huang F, Jiang X, Sorkin A. Tyrosine phosphorylation of the beta2 subunit of clathrin adaptor complex AP-2 reveals the role of a di-leucine motif in the epidermal growth factor receptor trafficking. J Biol Chem. 2003; 278(44):43411–43417. [PubMed: 12900408]

36. Sorkina T, Huang F, Beguinot L, Sorkin A. Effect of tyrosine kinase inhibitors on clathrin-coated pit recruitment and internalization of epidermal growth factor receptor. J Biol Chem. 2002; 277(30):27433–27441. [PubMed: 12021271]

37. Grossier JP, Xouri G, Goud B, Schauer K. Cell adhesion defines the topology of endocytosis and signaling. EMBO J. 2014; 33(1):35–45. [PubMed: 24366944]

38. Weng L, Enomoto A, Miyoshi H, Takahashi K, Asai N, Morone N, Jiang P, An J, Kato T, Kuroda K, Watanabe T, Asai M, Ishida-Takagishi M, Murakumo Y, Nakashima H, et al. Regulation of cargo-selective endocytosis by dynamin 2 GTPase-activating protein girdin. EMBO J. 2014; 33(18):2098–2112. [PubMed: 25061227]

39. Woelk T, Oldrini B, Maspero E, Confalonieri S, Cavallaro E, Di Fiore PP, Polo S. Molecular mechanisms of coupled monoubiquitination. Nat Cell Biol. 2006; 8(11):1246–1254. [PubMed: 17013377]

40. Henry AG, Hislop JN, Grove J, Thorn K, Marsh M, von Zastrow M. Regulation of endocytic clathrin dynamics by cargo ubiquitination. Dev Cell. 2012; 23(3):519–532. [PubMed: 22940114]

41. Ehrlich M, Boll W, Van Oijen A, Hariharan R, Chandran K, Nibert ML, Kirchhausen T. Endocytosis by random initiation and stabilization of clathrin-coated pits. Cell. 2004; 118(5):591–605. [PubMed: 15339664]
42. Taylor MJ, Perrais D, Merrifield CJ. A high precision survey of the molecular dynamics of mammalian clathrin-mediated endocytosis. PLoS Biol. 2011; 9(3):e1000604. [PubMed: 21445324]
43. Soohoo AL, Puthenveedu MA. Divergent modes for cargo-mediated control of clathrin-coated pit dynamics. Mol Biol Cell. 2013; 24(11):1725–1734. S1721–1712. [PubMed: 23536704]
44. Sanjana NE, Cong L, Zhou Y, Cunniff MM, Feng G, Zhang F. A transcription activator-like effector toolbox for genome engineering. Nat Protoc. 2012; 7(1):171–192. [PubMed: 22222791]
45. Dambournet D, Hong SH, Grassart A, Drubin DG. Tagging endogenous loci for live-cell fluorescence imaging and molecule counting using ZFNs, TALENs, and Cas9. Methods in enzymology. 2014; 546:139–160. [PubMed: 25398339]
46. Chen C, Zhuang X. Epsin 1 is a cargo-specific adaptor for the clathrin-mediated endocytosis of the influenza virus. Proc Natl Acad Sci U S A. 2008; 105(33):11790–11795. [PubMed: 18689690]
47. Boucrot E, Pick A, Camdere G, Liska N, Evergren E, McMahon HT, Kozlov MM. Membrane fission is promoted by insertion of amphipathic helices and is restricted by crescent BAR domains. Cell. 2012; 149(1):124–136. [PubMed: 22464325]
48. Sorkin A, Duex JE. Quantitative analysis of endocytosis and turnover of epidermal growth factor (EGF) and EGF receptor. Curr Protoc Cell Biol. 2010; Chapter 15(Unit 15):14. [PubMed: 20235100]
49. Rogstad SM, Sorkina T, Sorkin A, Wu CC. Improved precision of proteomic measurements in immunoprecipitation based purifications using relative quantitation. Anal Chem. 2013; 85(9): 4301–4306. [PubMed: 23517085]
50. Fortian A, Sorkin A. Live-cell fluorescence imaging reveals high stoichiometry of Grb2 binding to the EGF receptor sustained during endocytosis. J Cell Sci. 2014; 127(Pt 2):432–444. [PubMed: 24259669]

SYNOPSIS

We used RNA interference screen, mass-spectrometry and fluorescence microscopy to demonstrate that endocytosis of ubiquitylation-deficient mutants of the EGF receptor via clathrin coated pits is mediated by ubiquitylation. The model of EGF receptor endocytosis is proposed whereby two redundant mechanisms involving ubiquitylation and receptor interactions with AP-2 contribute to EGF receptor endocytosis in a stochastic fashion.

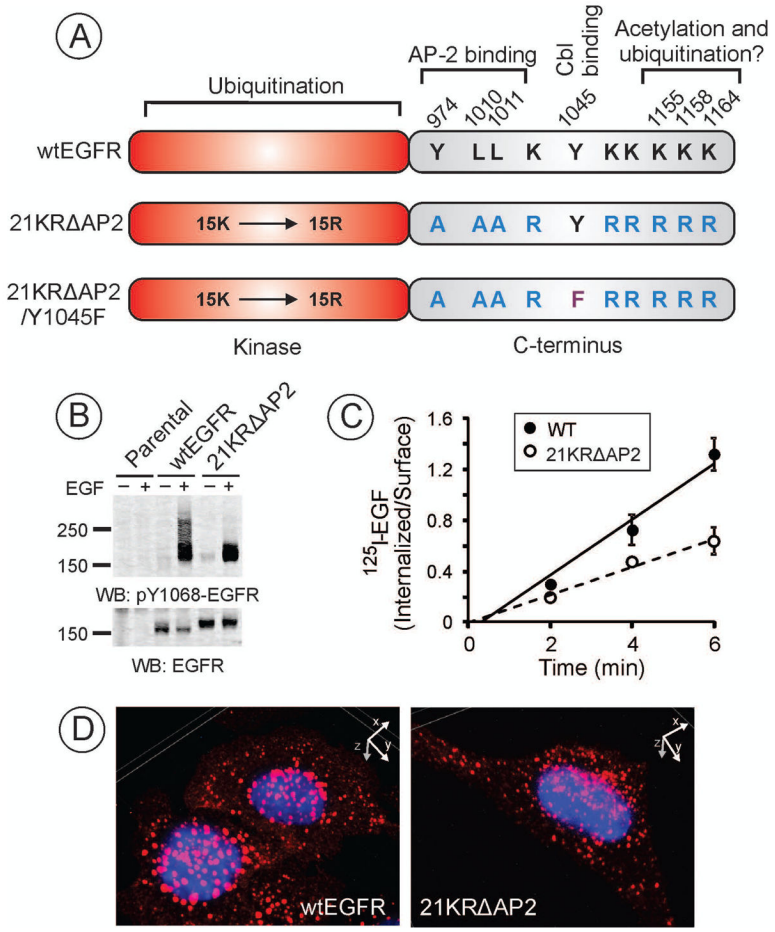

Figure 1. Internalization of EGFR mutants in HuTu-80 cells

(A) Schematic representation of the wild-type EGFR (wtEGFR) and EGFR mutants used in this study (only kinase and carboxyl-terminal domains are shown).

(B) HuTu-80 cells stably expressing wtEGFR or 21KRΔAP2, and parental HuTu-80 cells were incubated with 20 ng/ml EGF at 37°C for 5 min and lysed. The lysates were electrophoresed and analyzed by western blotting with antibodies to phosphorylated Tyr1068 (pY1068) of EGFR and EGFR (antibody 1005).

(C) HuTu-80 cells stably expressing wtEGFR or 21KRΔAP2 mutant were incubated with 1 ng/ml ^{125}I-EGF for the indicated times at 37°C, and the ratio of internalized and surface ^{125}I-EGF was determined and plotted against time.

(D) HuTu-80 cells stably expressing wtEGFR or 21KRΔAP2 mutant were incubated with 4 ng/ml EGF-Rh for 5 min at 37°C. After fixation, the cells were incubated with DAPI and mounted. 3D stack of images (30 planes, 0.2 μm spacing) of Rhodamine (red) and DAPI (blue) was acquired by the spinning-disk confocal microscope through 561 nm and DAPI channels. Fluorescence intensity settings are identical in these two images. Grid, 10 μm.

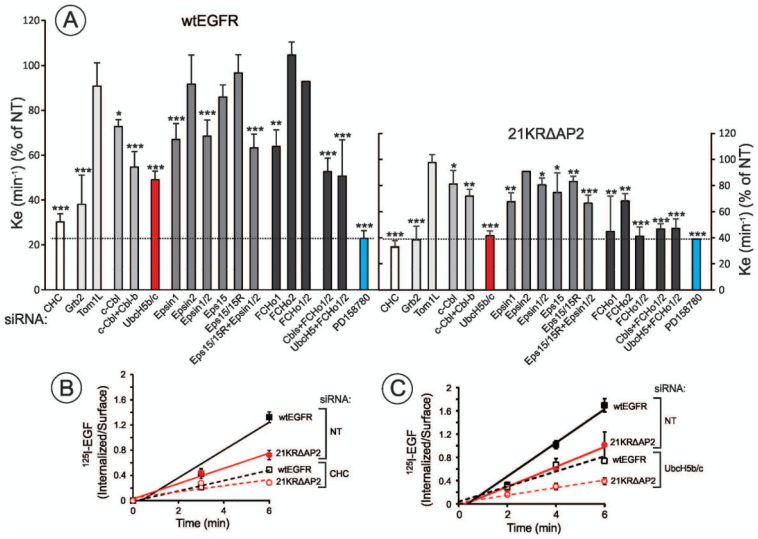

Figure 2. Effects of siRNAs on the internalization of wtEGFR and 21KRΔAP2

Internalization rates (ke) of wtEGFR and 21KRΔAP2 were measured using 1 ng/ml ^{125}I-EGF in cells transfected with non-targeting siRNA (NT) or various specifically targeted siRNA, or in the presence of EGFR tyrosine kinase inhibitor PD158780. The ratio of internalized and surface ^{125}I-EGF was determined, plotted against time and k_e values were calculated as described in “Methods”. Examples of western blots demonstrating the efficiency of protein knockdowns are presented in Supplemental Materials, Figure S1.

(A) Summary of ^{125}I-EGF internalization measurement in the presence or absence of siRNAs and an inhibitor. The data obtained in wtEGFR-expressing cells are expressed as the percentage of the internalization rate in cells treated with NT siRNA (mean +/− S.E.M.). The mean ^{125}I-EGF internalization rate in various clones of 21KRΔAP2-expressing cells was 58% of that value in wtEGFR-expressing cells. Therefore, the percentage values of 21KRΔAP2 internalization rates (right y-axis) were correspondently normalized. Dashed lines show the level of receptor kinase activity-independent internalization. *P<0.05; **P<0.01; ***P<0.005

(B) and **(C)** show examples of experiments demonstrating the effects of siRNAs to clathrin heavy chain (CHC) (**B**) or UbcH5b/c (**C**) on ^{125}I-EGF internalization by the wtEGFR and 21KRΔAP2 mutant.

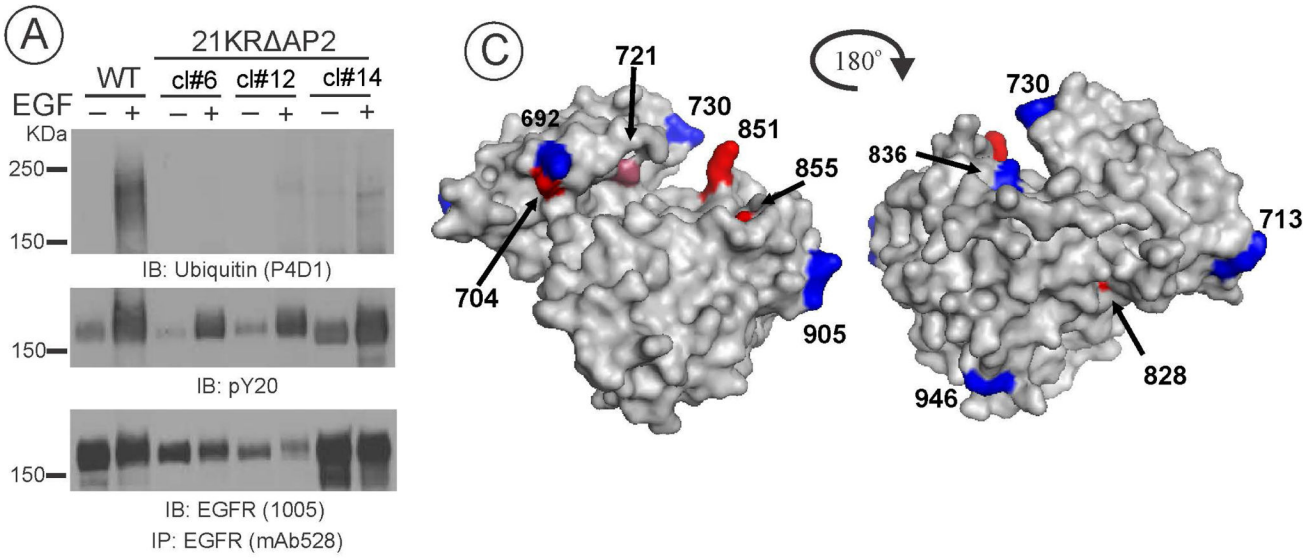

B

Site	Sequence	no EGF (peptide number)	Plus EGF (peptide number)	Spectra (page number*)
K704	VLGSGAFGTVYK^{GG}GLWIPEGER	1	1	22, 26
K721	IPVAIK^{GG}ELR	2	1	4, 27, 30
K828	TPQHVK^{GG}ITDFGLAR	2	2	5, 6, 28, 29
K851	EYHAEGGK^{GG}VPIK	1	4	1, 2, 25, 41, 43,
K855	VPIK^{GG}WMALESILHR	0	2	23, 24

*Page numbers refer to pages in the Supplemental Dataset

Figure 3. Ubiquitin-conjugation sites in the 21KRΔAP2 mutant

(A) wtEGFR and three clones of 21KRΔAP2 expressing HuTu-80 cells were stimulated or not with 20 ng/ml EGF for 5 min at 37°C, lysed, and EGFR was immunoprecipitated. 90% aliquots of the immunoprecipitates were analyzed by mass-spectrometry while 10% aliquots were probed with ubiquitin, phospho-tyrosine and EGFR antibodies by Western blotting.

(B) Mass-spectrometry analysis identified several tryptic diGly-modified peptides in the immunoprecipitates of the 21KRΔAP2 mutant (clone#14). The number of detected peptides is indicated in the middle column. References to the corresponding pages of the detailed spectral data of diGly-modified peptides found in wtEGFR and 21KRΔAP2 mutant presented in Supplemental Materials (Dataset) are listed in the far right column.

(C) The position of previously mapped and newly identified ubiquitin conjugation sites (all lysines) are shown on the structure of the activated kinase domain of EGFR (2GS2; surface density is shown) in blue and red, respectively.

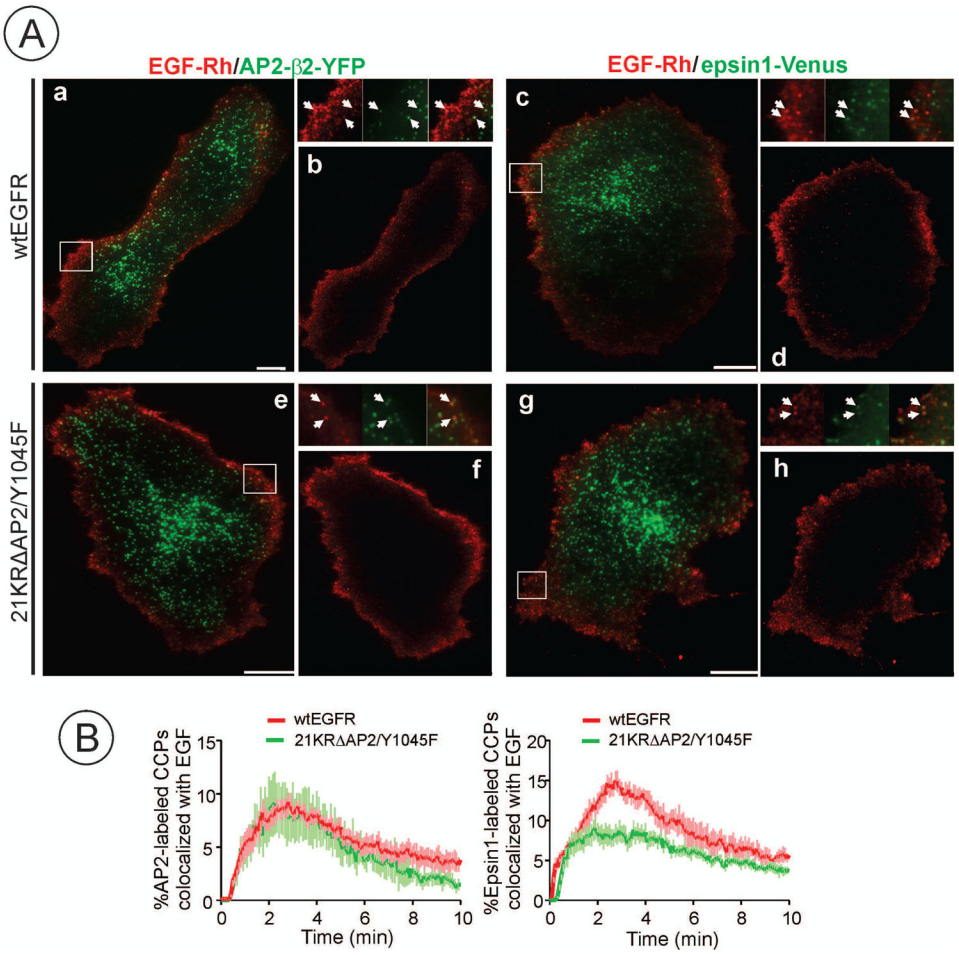

Figure 4. Recruitment of EGF-Rh in CCPs of HuTu-80 cells expressing wtEGFR or 21KRΔAP2/Y1045F mutant

(A) wtEGFR and 21KRΔAP2/Y1045F expressing cells were transiently transfected with β2-YFP or epsin1-Venus. After 2 days, time-lapse TIR-FM imaging of cells before and after cell simulation with EGF-Rh (2 ng/ml) was performed through 488 nm (YFP) and 561 nm channels (Rhodamine) at 37°C. Merged images (a, c, e, g) and EGF-Rh images (b, d, f, h) at a 3-min time-point after EGF-Rh stimulation are shown. Insets represent high magnification merged images of the regions marked by white rectangles. Arrows show examples of co-localization of EGF-Rh and CCP adaptor proteins. Scale bars, 10 μm.

(B) Time-course of the percentage of β2-YFP or epsin1-Venus labeled spots co-localized with EGF-Rh spots to the total number of β2-YFP or epsin1-Venus labeled spots was obtained in TIR-FM imaging experiments performed as in (***A***). Image analysis of 16800 CCPs from 46 cells was performed using Imaris 7.1 software. Error bars represent standard deviation of the mean.

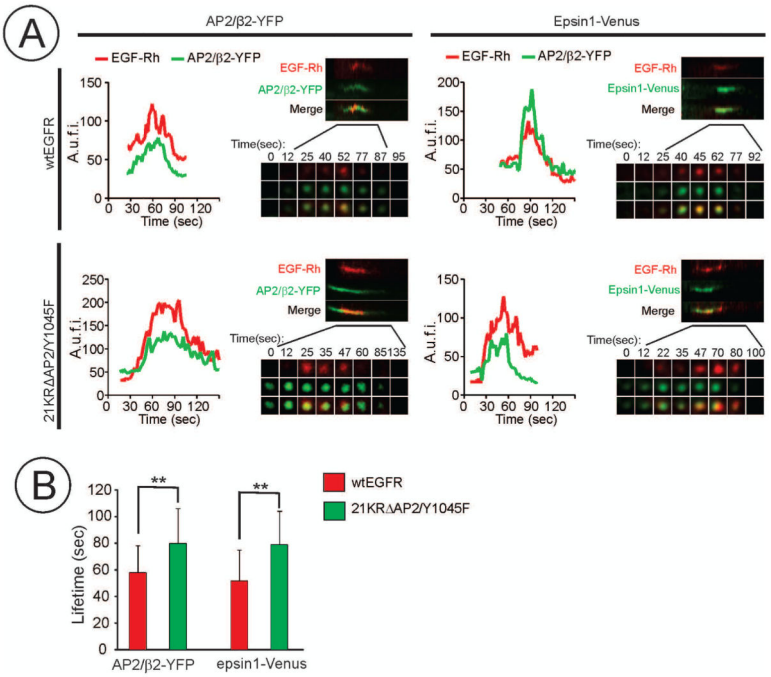

Figure 5. CCP lifetime analysis during internalization of EGF-Rh in HuTu-80 cells expressing wtEGFR or 21KRΔAP2/Y1045F mutant

wtEGFR and 21KRΔAP2/Y1045F expressing cells were transiently transfected with β2-YFP or epsin1-Venus. After 2 days, time-lapse TIR-FM imaging of cells before and after cell simulation with EGF-Rh (2 ng/ml) was performed as in Figure 4.

(A) Representative examples of fluorescence traces and kymographs from time-series of β2-YFP, epsin1-Venus and EGF-Rh imaging in CCPs which hosted a scission event. *A.u.f.i.*, arbitrary units of fluorescence intensity.

(B) Mean life-time values (+/−S.D.; n=20) of CCPs internalizing EGF-Rh were measured using β2-YFP and epsin1-Venus traces exemplified in (A). **p<0.01.

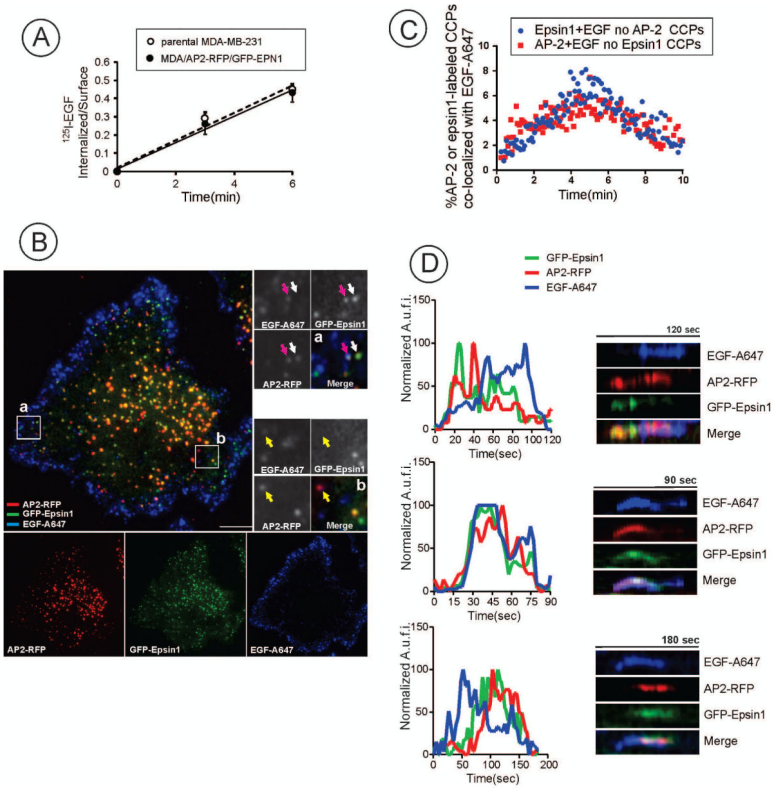

Figure 6. TIR-FM imaging of EGFR endocytosis in MDA-MB-231 cells expressing endogenously labeled epsin1 and AP2

(A) Internalization of ^{125}I-EGF by parental MDA-MB-231 and MDA-MB-231/AP2-RFP/GFP-EPN1 cells. The cells were incubated with 1 ng/ml ^{125}I-EGF for the indicated times at 37°C, and the ratio of internalized and surface ^{125}I-EGF was determined and plotted against time.

(B) Three-channel time-lapse TIR-FM imaging of cells before and after stimulation with EGF-A647 (20 ng/ml) was performed through 488 nm (GFP), 561 (RFP) and 640 (Alexa647) nm channels at 37°C. Single-channel and merged image at a 3-min time-point after EGF-A647 stimulation are shown. Insets represent high magnification merged images of the regions marked by white rectangles. Arrows show examples of co-localization of EGF-A647 with either Epsin1-GFP spots (white arrow), with both adaptor proteins (pink arrow) or AP2-RFP (yellow arrow). Scale bars, 10 μm.

(**C**) Percent of spots that were labeled only with either AP2-RFP or GFP-epsin1 and co-localized with EGF-Rh of the total number of spots singularly labeled with AP2-RFP or GFP-epsin1 was measured in time-series of TIR-FM imaging performed as in (***A***). Image analysis of 805 tracks from 5 cells was performed using Imaris 7.1 software. Mean values for each time point with error bars representing standard deviation of the mean are plotted against time.

(**D**) Representative examples of fluorescence traces and kymographs from time-series of AP2-RFP, GFP-epsin1 and EGF-A647 imaging in CCPs which hosted a scission event. TIR-FM imaging was performed as (***B***). ***A.u.f.i.***, arbitrary units of fluorescence intensity.

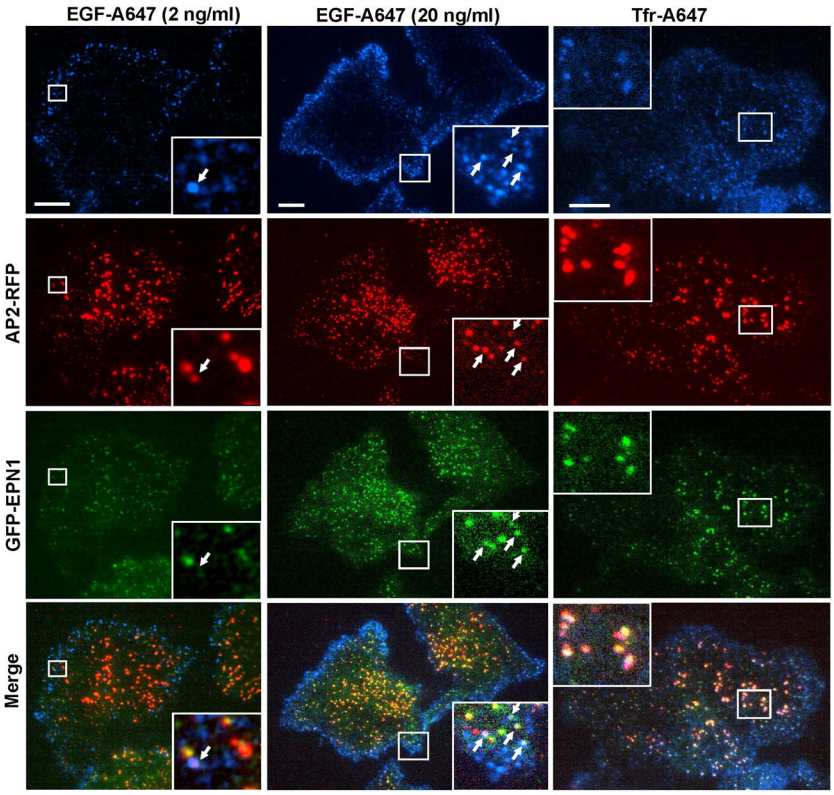

Figure 7. TIR-FM imaging of EGF and transferrin endocytosis in MDA-MB-231/AP2-RFP/GFP-EPN1 cells

Three-channel TIR-FM imaging of cells incubated with EGF-A647 (2 or 20 ng/ml) or Trf-A647 (5 μg/ml) at 37°C was performed as in Fig. 6. Single-channel and merged images at an 80-sec time-point after ligand addition are shown. Insets represent high magnification images of the regions marked by white rectangles. Arrows show examples of co-localization of EGF-A647 or Tfr-A647 with AP2-RFP and/or Epsin1-GFP. Scale bars, 10 μm.